# Gamma Decays of the First $T=\frac{3}{2}$ States in $^9$Be and $^9$B

J. C. Adloff, K. H. Souw, and C. L. Cocke*†
*Institut de Recherches Nucléaires, Strasbourg, France*
(Received 1 December 1970)

The reactions $^7$Li($^3$He,$p$)$^9$Be(14.39 MeV)($\gamma$) and $^7$Li($^3$He,$n$)$^9$B(14.67 MeV)($\gamma$) have been used to study the $\gamma$-decay modes of the first $T=\frac{3}{2}$ states in $^9$Be and $^9$B. $\gamma$ spectra from a NaI detector were recorded in coincidence with proton energy spectra from the $^7$Li($^3$He,$p$) reaction, and with neutron time-of-flight spectra from the $^7$Li($^3$He,$n$) reaction. In addition, the singles $\gamma$ spectrum from the 14.39-MeV state in $^9$Be was studied using a Ge-Li detector. The $\gamma$ spectrum from the Ge-Li detector gives the branching ratio $\Gamma_{\gamma(2.43)}/\Gamma_{\gamma 0}=1.19\pm0.16$ for the decay of the first $T=\frac{3}{2}$ state in $^9$Be. From the $\gamma$-$n$ coincidence spectrum below threshold for production of $^9$B(14.67 MeV) a $\gamma$ decay from $^9$Be(14.39 MeV) to a state in $^9$Be at $E_x=2.9\pm0.25$ MeV was found. The total width of this state was found to be $\Gamma=1.0\pm0.25$ MeV. A measurement of the strength of this $\gamma$ branch relative to that to $^9$Be(2.43 MeV) yields $\Gamma_{\gamma(2.9)}/\Gamma_{\gamma(2.43)}=0.30\pm0.04$. From the $\gamma$-$n$ spectra above the $^9$B(14.67 MeV) threshold a $\gamma$-decay spectrum from the (14.67-MeV) state in $^9$B was obtained which shows consistency with the branching ratios obtained for $^9$Be(14.39 MeV). Combining our branching ratios with previously available information allows us to present a best set of radiative widths from the first $T=\frac{3}{2}$ levels in $^9$Be and $^9$B. From the coincidence spectra the value for $\Gamma_{\gamma 0}/\Gamma_{tot}$ is found to be $0.021\pm0.004$ for $^9$Be(14.39 MeV). The ratios of the total widths $\Gamma_{tot}(^9\text{Be}(14.39\text{ MeV}))/\Gamma_{tot}(^9\text{B}(14.67\text{ MeV}))$ is deduced as $1.23^{+0.54}_{-0.43}$. When combined with the value for $\Gamma_{\gamma 0}(^9\text{Be (14.39 MeV)})$, these ratios yield $\Gamma_{tot}=0.50\pm0.1$ keV ($^9$Be) and $0.4^{+0.14}_{-0.18}$ keV ($^9$B) for the total widths of the two states.

## 1. INTRODUCTION

The recognition that, above mass 5, the first $T=\frac{3}{2}$ levels in the $4n+1$ series of light nuclei are bound with respect to isospin-allowed particle decays has lent special interest to their study in recent years. With the exception of mass 17, $\gamma$ decays from these states have been studied throughout the $1p$ and $s$-$d$ shells. Experimentally, the detection of these $\gamma$ rays is facilitated by the isospin retardation of particle decays from the $T=\frac{3}{2}$ states and by the high energy of the emitted photons. From a theoretical point of view, such $\gamma$ decays satisfy several criteria which make them an ideal testing ground for nuclear model calculations. Both the $T=\frac{3}{2}$ levels and the $T=\frac{1}{2}$ levels to which they decay are usually narrow states. They are often thought to be describable in terms of rather simple configurations and structure, and the identification of the model state with the experimental one is usually unambiguous.

In addition to offering nuclear states whose major components may prove easy to explain, low-lying $T=\frac{3}{2}$ states offer good opportunities for probing isospin impurities in light nuclei. Both the isospin-forbidden particle decays[1,2] and the allowed $\gamma$ decays[3-5] have been studied extensively to this end. Studies in mass 13 revealed that the electromagnetic transition rates from the first $T=\frac{3}{2}$ states in $^{13}$N (at 15.03 MeV) and $^{13}$C (at 15.07 MeV) to the ground state[4,6,7] and first few excited states[5] are consistent with the prediction that $\Delta T=1$ radiative transitions in conjugate nuclei have equal strengths.[8] The total width of the $^{13}$N(15.03 MeV) state[1,5,9,10] was found to be considerably less than that of the $^{13}$C(15.07 MeV) state.[1,5,11] This adds to the experimental evidence indicating that the isospin impurities are $z$ dependent.

In the present study we have undertaken measurement of branching ratios from the first $T=\frac{3}{2}$ levels in $^9$Be and $^9$B. In addition we wished to see if the variation with $Z$ of the total widths observed in $A=13$ was reproduced in $A=9$. To this end we have measured $\Gamma_{\gamma 0}/\Gamma_{tot}$ for $^9$Be and the ratio of total widths in $^9$Be and $^9$B which, when combined with a previously known value for $\Gamma_{\gamma 0}$, allow us to extract values for the two total widths.

The $^9$Be(14.39 MeV) $\gamma$-decay spectrum revealed a weak branch to a broad level at about 2.9 MeV in excitation. There has long been a very insistent prediction by the shell model that a $\frac{1}{2}^-$ level should exist in this region.[12-14] Macefield, Wakefield, and Wilkinson[15] and Chen, Tombrello, and Kavanagh (CTK)[16] have found that a level with the appropriate character is fed by the $\beta$ decay of $^9$Li. In view of the similarity of the $M1$ and Gamow-Teller $\beta$-decay operators, one might expect the $M1$ $\gamma$ decay from $^9$Be(14.39 MeV), the analog of the $^9$Li ground state, to feed this state with a branch comparable to that found in the $^9$Li $\beta$ decay. For this reason we have spent considerable effort trying to separate this weak decay mode in our spectra.

The first $T=\frac{3}{2}$ states in $^9$Be and $^9$B have excitations of $14.392\pm0.005$ and $14.670\pm0.016$ MeV, re-

spectively[17] (Fig. 1). $\gamma$ decay from these states has previously been seen by Griffiths[3] in the singles spectrum from $^7$Li + $^3$He. He was able to detect decays to the ground and 2.43-MeV states in $^9$Be and extracted $\Gamma_{\gamma 0}/\Gamma_{tot} = 0.023 \pm 0.005$. Combined with $\Gamma_{\gamma 0} = 10.5 \pm 1.5$ eV,[18] this yields $\Gamma_{tot} = 0.46 \pm 0.17$ keV. Evidence was seen for a similar decay scheme from $^9$B(14.67 MeV), though it was difficult to distinguish decays from $^9$B from those from $^9$Be. The spin assignments of $\frac{3}{2}^-$ are taken from the $\frac{3}{2}^-$ spin of the ground state of $^9$Li.

## 2. EXPERIMENTAL PROCEDURE

A $^3$He$^{++}$ beam of typically 50 nA was delivered by the 5.5-MeV Van de Graaff of the Centre de Recherches Nucléaires onto a beam spot whose diameter was about 2 mm. Targets of metallic lithium, enriched to 99.99% in $^7$Li, were evaporated onto backings of Ni or Ta in a separate vacuum system and transferred under vacuum to the target chamber, using a specially constructed target holder. Details of beam, target thickness, and backing are described in individual sections.

### A. $p$-$\gamma$ Coincidence Spectra

The reaction $^7$Li($^3$He, $p$)$^9$Be was used to populate the 14.39-MeV state in $^9$Be, and the ensuing $\gamma$ rays were detected in coincidence with the protons. Our primary effort was directed toward obtaining a clean spectrum from the $^9$Be(14.39 MeV) decay. The requirement that the $\gamma$ ray appear in coincidence with a proton of the appropriate energy made unambiguous the identification of the emitting state and eliminated much of the background which appeared in the singles spectra of Griffiths.[3] Since Griffiths had measured $\Gamma_{\gamma 0}/\Gamma_{tot}$ for $^9$Be(14.39 MeV), we controlled our normalization in order to be able to extract this ratio from our data as well, using a singles proton spectrum and our calculated coincidence efficiency. A comparison of our value with that of Griffiths served as a check on the consistency of our experiment with his. As discussed in Ref. 5 the detection of the proton at 0° and of the $\gamma$ ray at a zero of $P_2(\cos\theta)$ eliminates the need to do a detailed angular correlation in order to determine this ratio. For this reason we chose to use $\theta_p = 0°$, $\theta_\gamma = 125°$.

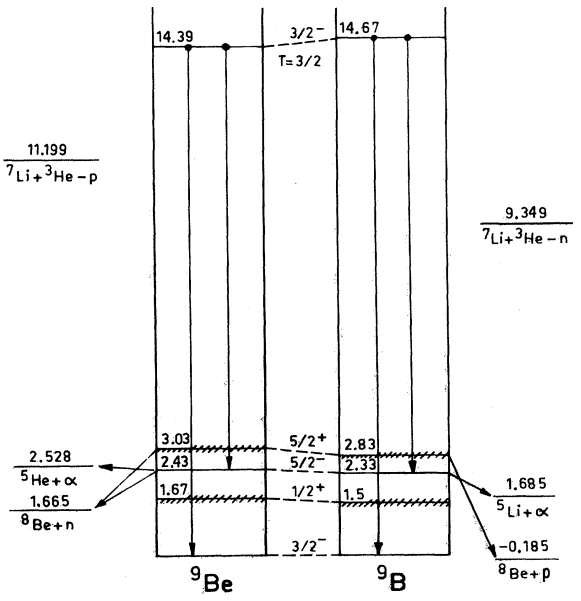


FIG. 1. Partial energy-level diagram for $^9$Be and $^9$B. The ground states have been aligned.

A $^7$Li target of 200 $\mu$g/cm$^2$ (75 keV for a 10-MeV $^3$He) was evaporated onto a 50-$\mu$ tantalum backing. The tantalum was thick enough to range out the beam while letting the protons pass through into the detector. A 1000-$\mu$-thick surface-barrier detector collimated by a 7-mm-diam circular aperture 2 cm from the beam spot was used as the proton detector. $\gamma$ rays were detected in a 12.7-cm $\times$ 10.16-cm NaI crystal coupled to an XP-1040 photomultiplier; the face of the crystal was located 7.3 cm from the target. A 350-$\mu$-thick surface-barrier detector situated at $\theta = -140°$, collimated by a 3-mm-diam circular aperture 3.3 cm from the target and covered by 100 $\mu$ of aluminum, was used as a monitor. The deuteron group from the reaction $^7$Li($^3$He, $d$)$^8$Be(g.s.) stood out clearly in the monitor spectrum and was used to normalize the coincidence spectrum to the singles proton spectrum taken later. Two-dimensional spectra of proton energy vs $\gamma$ energy were stored when the proton arrived within 20 nsec of the $\gamma$ ray.

In Fig. 2(a), we show a coincidence spectrum of proton energy vs $\gamma$-ray energy, for a bombarding energy of 10 MeV. The horizontal line centered at proton channel 13 corresponds to $\gamma$ decay from the 14.39-MeV state in $^9$Be. Heavily populated spots at (proton channel, $\gamma$ channel) of (8, 30) and (28, 54) are produced by the $^{12}$C($^3$He, $p$)$^{14}$N($\gamma$) reaction from carbon contamination in the target. A projection of the $^9$Be(14.39 MeV) $\gamma$-decay spectrum, after subtraction of the appropriately normalized random coincidences, is shown in Fig. 2(b). $\gamma$ decays to the ground state and to the 2.43-MeV state of $^9$Be contribute peaks centered at about channels 107 and 89, respectively.

The spectral response of the NaI crystal-photomultiplier combination to monoenergetic photons of energies between 10 and 17 MeV was measured using the reactions $^{11}$B($p, \gamma$), $^{11}$B($d, n$)$^{12}$C($\gamma$), and $^{15}$N($p, \gamma$). Using these curves, an attempt was made to describe the spectrum of Fig. 2(b) as the sum of two $\gamma$ rays whose energies were 14.39 MeV

and 14.39–2.43 MeV. The solid line shows the resultant ground-state contribution. Attempts to describe the remaining spectrum with a curve corresponding to the expected response from a 11.96-MeV $\gamma$ ray produced curves which visibly failed to account for the data (see Sec. C).

### B. Singles Proton Spectra

In order to determine $\Gamma_{\gamma 0}/\Gamma_{\text{tot}}$ for $^{9}$Be(14.39 MeV), it was necessary to be able to determine the number of times the 14.39-MeV level had been populated during the accumulation of a $p$-$\gamma$ coincidence spectrum.

The singles spectrum from $^{7}$Li($^{3}$He,$p$)$^{9}$Be, under conditions described above for the $p$-$\gamma$ measurements, did not allow clean separation of the proton group corresponding to the 14.39-MeV state, due to the poor energy resolution introduced by the thick target and by straggle of the protons through the tantalum target support. It was therefore necessary to use a different experimental configuration to obtain the necessary singles spectrum.

A target of 60 $\mu$g/cm$^2$ $^{7}$Li was evaporated onto a 0.1-$\mu$ nickel foil. The protons were detected in an ($E$-$\Delta E$) silicon surface-barrier telescope consisting of a 29-$\mu$-thick $\Delta E$ detector followed by a 1000-$\mu$ full-energy detector. The telescope was collimated by a circular aperture 1 mm in diameter located at 3.5 cm from the target spot. The same monitor arrangement was used for this part of the experiment as was used during the $p$-$\gamma$ coincidence runs, thus allowing straightforward normalization of singles to coincidence spectra.

Fig. 3(a) shows a sample proton spectrum. The proton group from the 14.39-MeV state in $^{9}$Be stands just below a large group of protons which originates from the elastic scattering of contaminant hydrogen out of the target.

The appearance of numerous peaks from the reaction $^{12}$C($^{3}$He,$p$)$^{14}$N led us to take a comparison spectrum using a carbon foil as a target [Fig. 3(b)]. Contributions from contaminant groups in $^{14}$N were substracted when necessary from the $^{9}$Be(14.39 MeV) peak; their contribution never

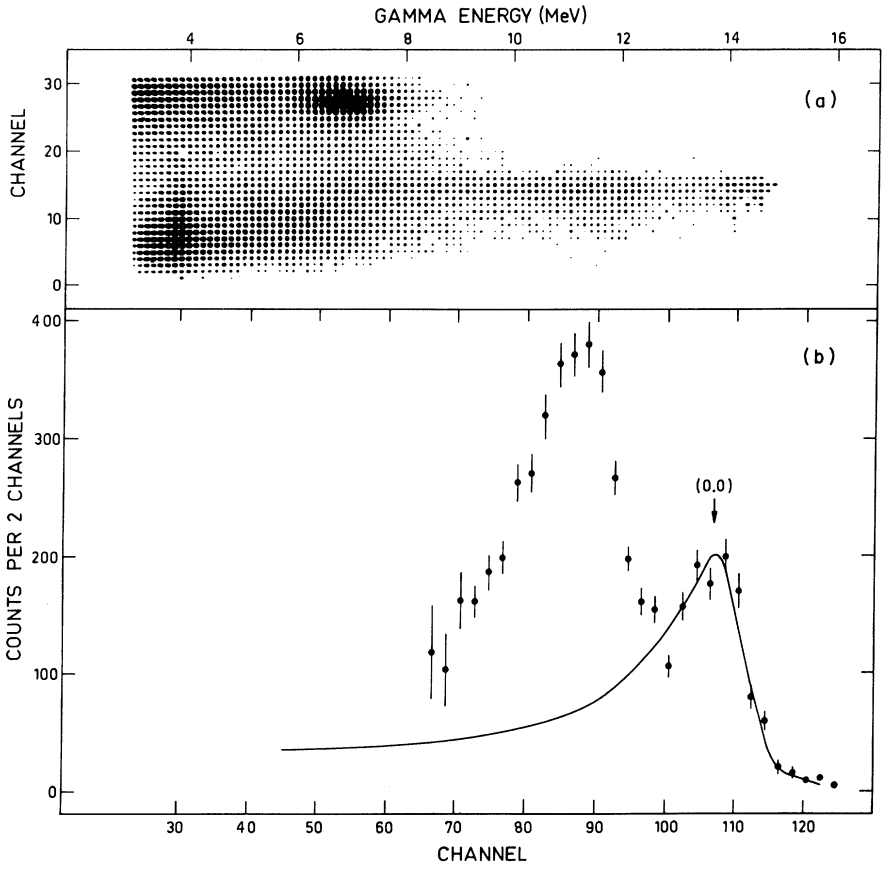


FIG. 2. (a) Particle energy vs $\gamma$-ray energy spectrum from $^{7}$Li + $^{3}$He, $E(^{3}\text{He}) = 10$ MeV, $\theta_p = 0°$, $\theta_\gamma = 125°$. Events from $^{7}$Li($^{3}$He,$p$)$^{9}$Be(14.39 MeV)($\gamma$) appear at proton-energy channel 13. (b) High-energy portion of the summed $\gamma$ spectrum from the decay of the 14.39-MeV, $T = \frac{3}{2}$ level in $^{9}$Be.

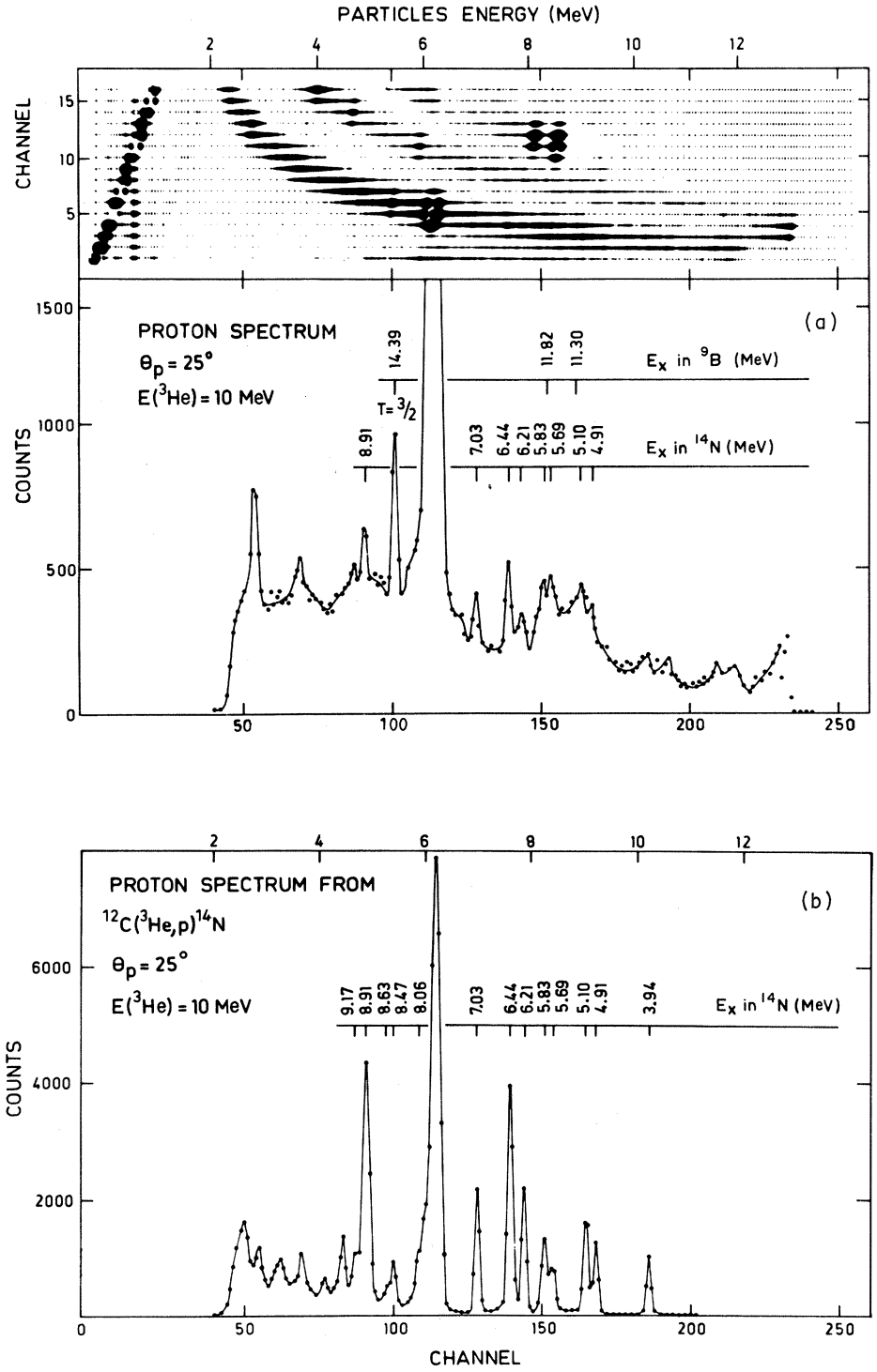


FIG. 3. (a) Particle energy loss vs full energy spectrum from $^7$Li + $^3$He, $E(^3\text{He}) = 10$ MeV, $\theta_p = 25°$, showing proton, deutron, and triton lines. Deuteron groups at energy loss channel 14 and 10 are from $^{16}$O($^3$He,$d$)$^{17}$F(g.s.) and $^{12}$C($^3$He,$d$)-$^{13}$N(g.s), respectively. Heavily populated triton groups at channel 11 and 10 are from $^7$Li($^3$He,$t$)$^7$Be(g.s. and 0.431-MeV state). A sum over proton line is shown. Proton group at full-energy channel 125 is from $^1$H($^3$He,$p$). Hydrogen, carbon, and oxygen are target contaminants. (b) Summed proton spectrum using a 15-$\mu$g/cm$^2$ self-supporting $^{12}$C target in the same experimental conditions as above. Contamination from $^{12}$C($^3$He,$p$) in the $^7$Li($^3$He,$p$)$^9$Be(14.39 MeV) group [Fig. 3(a)] are evaluated using the $^{12}$C($^3$He,$p$)$^{14}$N(8.91 MeV) group appearing in both proton spectra (a) and (b).

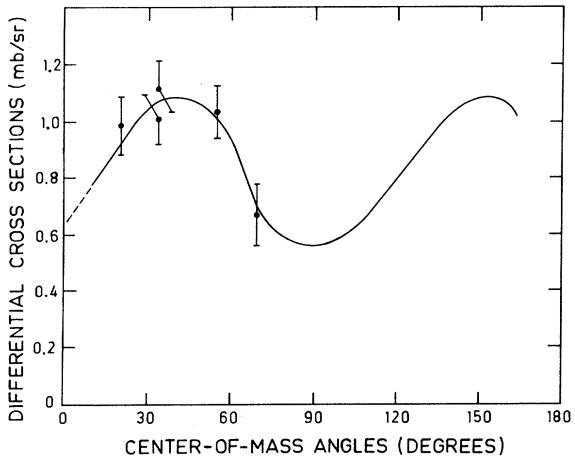


FIG. 4. Differential cross sections vs center-of-mass angles from $^{7}$Li($^{3}$He,$p$)$^{9}$Be(14.39 MeV), $E(^{3}\mathrm{He})=10$ MeV. The solid line is from Ref. 19. The chosen extrapolation is shown in dashed line.

exceeded 5% of the main peak.

The proton yield from $^{7}$Li($^{3}$He,$p$)$^{9}$Be(14.39 MeV) could not be measured directly at 0°, the angle used for the coincidence measurements. An angular distribution of these protons at $E(^{3}\mathrm{He})=10$ MeV had been previously measured by Lynch, Griffiths, and Lauritsen,[19] however. Using our points, measured at angles greater than 15°, and their shape for the angular distribution, as shown in Fig. 4, we extrapolated the proton yield into the region used for the coincidence measurements ($\theta_p = 0-7°$ cm). Our method for determining the absolute efficiency of the NaI detector, which we needed in order to calculate our over-all coincidence efficiency, has been described previously.[5]

Our results for the number of $\gamma$ rays per proton from $^{9}$Be(14.39 MeV) are $\Gamma_{\gamma 0}/\Gamma_{\mathrm{tot}} = 0.021 \pm 0.004$, in excellent agreement with the value $0.023 \pm 0.005$ found by Griffiths.[3] An average of the two results, when combined with $\Gamma_{\gamma 0} = 10.5 \pm 1.5$ eV,[18] yields

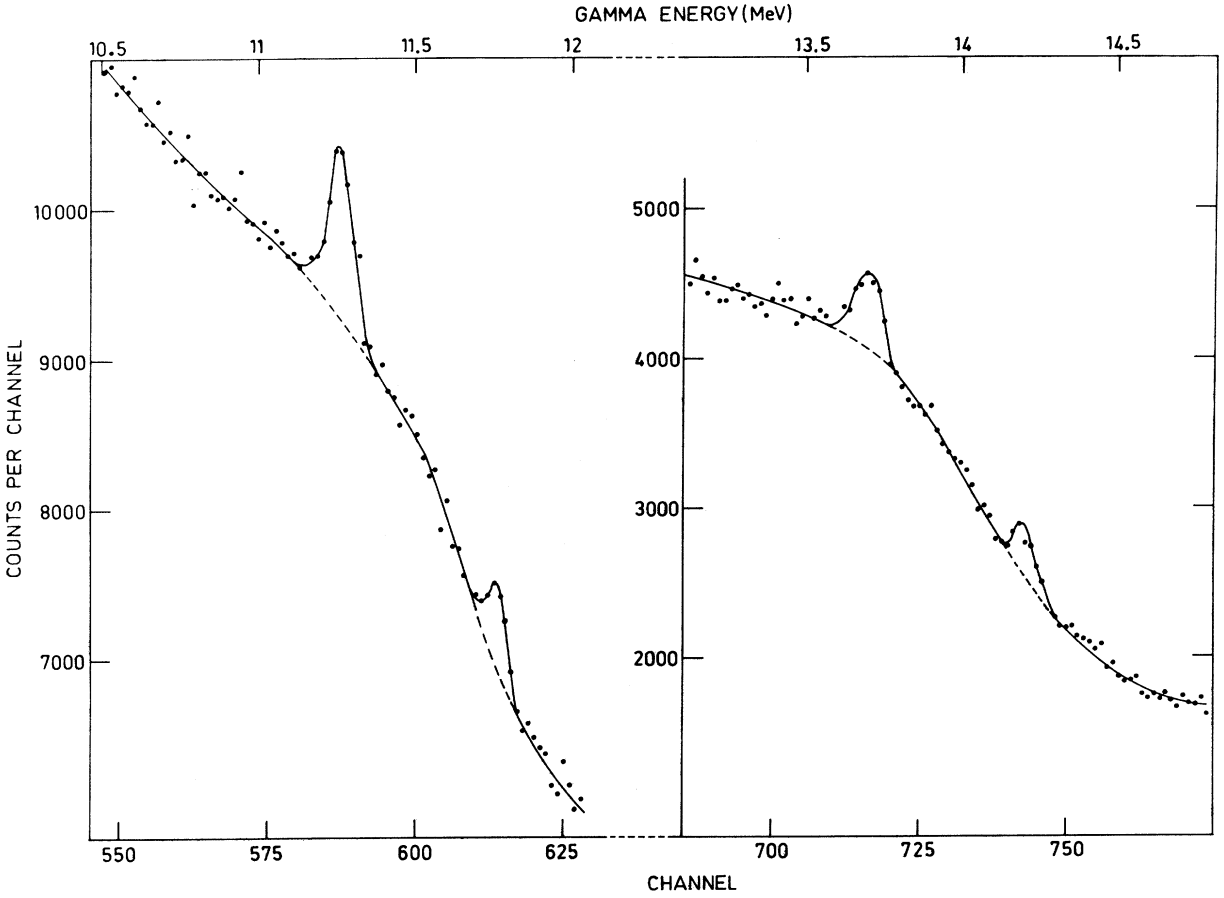


FIG. 5. High-energy $\gamma$-Ge-Li spectrum from $^{7}$Li+$^{3}$He, $E(^{3}\mathrm{He})=5.5$ MeV, $\theta_\gamma = 0°$. First and second escape peaks of the $\gamma$ rays decaying from $^{9}$Be(14.39 MeV) to ground- and 2.43-MeV states are, respectively, at channels 743–714 and 612–584.

$\Gamma_{tot} = 0.50 \pm 0.10$ keV for the 14.39-MeV state in $^9$Be.

### C. Ge-Li Spectrum

Our inability to describe the $\gamma$-decay spectrum from $^9$Be(14.39 MeV) in terms of decays to the ground and 2.43-MeV states alone led us to try to measure the ratio $\Gamma_{\gamma(2.43)}/\Gamma_{\gamma 0}$ using a Ge-Li detector. This spectrum should show as peaks only decays to the sharp ground and 2.43-MeV states. A coaxial detector having a nominal sensitive volume of 95 cm$^3$, an outer diameter of 4 cm, and length of 8 cm, built at Strasbourg by Société d'Applications Industrielles de la Physique, was used for this purpose. The detector was placed at 0°, its axis coincident with that of the beam, with the surface of the germanium crystal 3.1 cm from the target. A target of 400 $\mu$g/cm$^2$ $^7$Li(240 keV to a 5.5-MeV $^3$He) was bombarded by a 5.5-MeV $^3$He beam. This beam energy is 660 keV above the threshold for the reaction $^7$Li($^3$He, $p$)-$^9$Be(14.39 MeV) and below threshold for $^7$Li($^3$He, $n$)-$^9$Be(14.67 MeV). Although a higher bombarding energy would have increased the yield of $\gamma$ rays from $^9$Be(14.39 MeV), it also would have increased the Doppler spread caused by the distribution in velocities which the departing protons leave to the recoiling $^9$Be nucleus. The size of this spread is already 100 keV (base width) for the ground-state transition at $E(^3\text{He}) = 5.5$ MeV and is the limiting factor in determining the resolution obtained in the Ge-Li spectrum. The 5.5-MeV bombarding energy was chosen as a compromise between yield and resolution.

Fig. 5 shows a part of the spectrum resulting from 12 h of bombardment at 40-nA beam current. First and second escape peaks corresponding to transitions from the 14.39-MeV state to the ground and 2.43-MeV states of $^9$Be are in evidence. In order to use the areas from these peaks to determine $\Gamma_{\gamma(2.43)}/\Gamma_{\gamma 0}$, the relative efficiency of the Ge-Li detector must be known for photon energies of 14.39 and 11.96 MeV. A relative efficiency curve for the detector was measured as a function of $\gamma$ energy using the reactions $^{13}$C + $p$, $^{15}$N + $p$, $^{11}$B + $p$, and $^{11}$B + $d$ to produce sufficiently monoenergetic photons. The NaI detector, described in Sec. 2B, was used as a standard whose efficiency could be calculated. The procedure followed was to measure several points on the efficiency curve immediately following the recording of the $^9$Be spectrum, changing only target and beam but

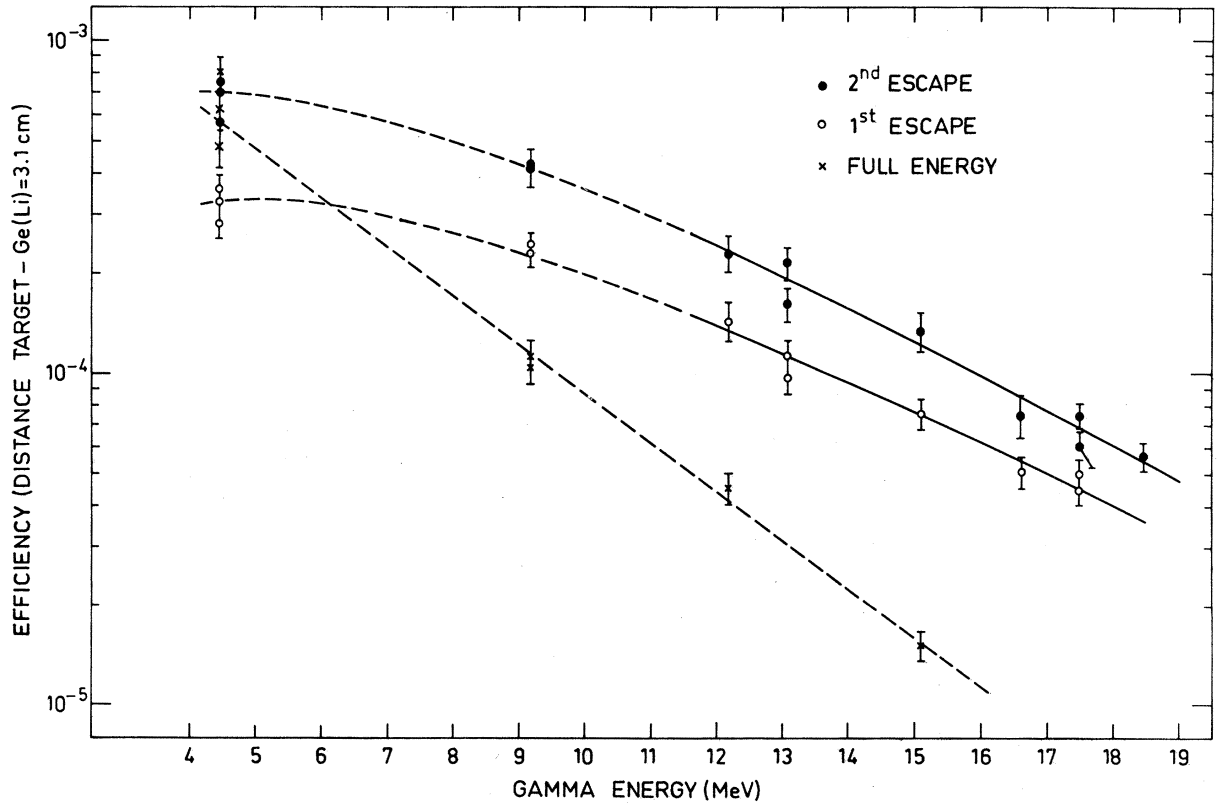


FIG. 6. Absolute efficiencies for the 95-cc Ge(Li) counter. The distance from target to Ge(Li) front face is 3.1 cm.

without disturbing the geometry. Resulting curves are shown in Fig. 6. Making use of these curves to extract the relative yields of the ground and 2.43-MeV states transitions from Fig. 5, we find $\Gamma_{\gamma(2.43)}/\Gamma_{\gamma 0} = 1.19 \pm 0.16$.

Very different angular distributions for the $\gamma$ rays could render this conclusion invalid. Griffiths found both distributions to be approximately isotropic, however. A Ge-Li spectrum taken at $\theta_\gamma = 90°$ yielded $\Gamma_{\gamma(2\ 43)}/\Gamma_{\gamma 0} = 1.07 \pm 0.25$ in good agreement with the 0° value given above. We are thus given confidence that our neglect of possible angular-distribution effects has not introduced large errors into our final branching ratio.

### D. $n$-$\gamma$ Coincidence Spectra Relevant to $^9$Be

Using the branching ratio for $\Gamma_{\gamma(2.43)}/\Gamma_{\gamma 0}$ found above, we returned to the $\gamma$ spectrum of Fig. 2(b) to try to explain the observed spectral shape as shown in Fig. 11. The result of subtracting the contributions from decay to the ground state (I) and to the 2.43-MeV state (II), whose intensity relative to the ground-state intensity was taken from the above branching ratio, was a spectrum which appeared to represent a decay to a state at about 3 MeV in $^9$Be (III) of intensity about 25% of that to the 2.43-MeV state.

There are two levels near this region of excitation in $^9$Be to which such a decay might go. The first is the $\frac{5}{2}^+$, $T = \frac{1}{2}$ level at 3.03 MeV ($\Gamma$ = 265 keV), to which a transition from the $\frac{3}{2}^-$, $T = \frac{3}{2}$ level at 14.39 MeV could go by $E1$ photon emission. In a shell-model description this level would presumably contain primarily the configuration $(1s)^4$ $(1p)^4$ $(2s, 1d)$, coupled to $T = \frac{1}{2}$. A transition between a pure $1p$-shell state with $T = \frac{3}{2}$ and such a configuration is not possible, since it involves changing simultaneously a particle orbit and the isospin coupling of the remaining eight particles. Thus to the extent that the $\frac{3}{2}^-$, $T = \frac{3}{2}$ and $\frac{5}{2}^+$, $T = \frac{1}{2}$ states are of the above configurations, there should be no $E1$ matrix element between them. The second is the recently found $\frac{1}{2}^-$ level, to which $M1$ decay should be of an intensity comparable to that to the $\frac{5}{2}^-$, 2.43-MeV level. The $\frac{5}{2}^+$ level is known to decay $87 \pm 13\%$ to $^8$Be(g.s.).[20] Because of its large predicted reduced width for neutron emission to Be(g.s.) and the large energy available for this decay relative to that available for decay to the 2.9-MeV state of $^8$Be, the $\frac{1}{2}^-$ level is expected to decay primarily to Be(g.s.). Experimentally, CTK[16] find that at least 60% of the decay is via this mode.

In order to separate more clearly the decay branch to the 3-MeV level(s) and in hopes of shedding further light on the excitation and width of the level, we undertook a $\gamma$-$n$ measurement analogous to the $\beta$-$n$ coincidence technique used in studying the $^9$Li decay. The reaction $^7$Li($^3$He, $p$) was used to feed the 14.39-MeV level in $^9$Be, and the $\gamma$ rays

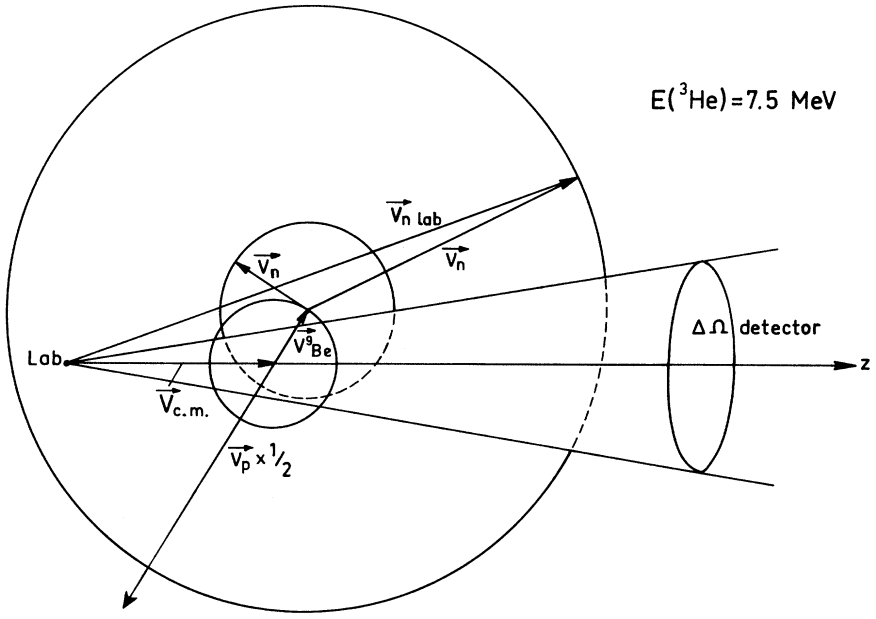


FIG. 7. Velocity diagram for $^7$Li($^3$He,$p$)$^9$Be*($\gamma$)$^9$Be*($n$). The recoil imparted by $\gamma$ rays to the $^9$Be* nucleus is neglected. Dashed lines in neutron velocity spheres show that low-energy neutrons are detected with better efficiency than high-energy ones. The neutron velocities $V_n$ are represented in the $^9$Be* system.

from this state were detected in coincidence with the neutron resulting from the subsequent breakup of lower $^9$Be levels fed by the $\gamma$ decay. Since both the $\gamma$ energy and the neutron flight time depend on the state to which the $\gamma$ decay goes, a coincident measurement of $\gamma$ energy and neutron flight time provides more information to be used in the separation of decays to the 2.43- and ~3-MeV states in $^9$Be than does either spectrum alone.

A 200-$\mu$g/cm$^2$ $^7$Li target on a 0.1-mm tantalum support was bombarded by a $^3$He beam at an energy of 7.5 MeV, just below the $^9$B(14.67 MeV) threshold. The $\gamma$ rays were detected at $\theta_\gamma = 125°$ using the NaI detector described in Sec. 2B. The neutrons were detected at 0° in a 5.08-cm-thick × 12.7-cm-diam Naton 136 plastic scintillator coupled to a 58 AVP photomultiplier. A flight path from target to scintillator face of 34.2 cm was used.

The velocity diagram for the process $^7$Li($^3$He,$p$)-$^9$Be (14.39 MeV)($\gamma$)$^9$Be*($n$)$^8$Be is shown in Fig. 7. Even if the process proceeds through well-defined excitations in $^9$Be and $^8$Be, the recoil momentum imparted to the $^9$Be by the proton will produce a distribution of neutron velocities at a given laboratory neutron angle. While the resultant neutron time-of-flight spectrum loses some detail from this effect, it was not sufficiently degraded to lose the features we sought.

Figure 8 shows a spectrum of neutron flight time vs $\gamma$ energy resulting from 12 h of measurement at 50 nA of beam current. A line due to $\gamma$-$\gamma$ coincidences appears near time channel 50. The time region marked I delineates the area in which events from $^7$Li($^3$He,$p$)$^9$Be(14.39 MeV)($\gamma$)$^9$Be(2.43) ($\alpha + \alpha + n$)$^{16}$ should occur and the spectrum is dominated by evidence for this decay mode. If a level at 3 MeV in $^9$Be is fed, and if the subsequent $n$ decay is to $^8$Be(g.s.), corresponding events should fall mainly in region II. Projections of these two regions on the $\gamma$-energy axis are shown in Fig. 9. Solid curves are shapes expected for $\gamma$ decay to $^9$Be(2.43) and to $^9$Be(2.9; $\Gamma$ = 1 MeV) for regions I and II, respectively.

Figure 10 displays a projection of events above $\gamma$-energy channel 30 onto the neutron time-of-

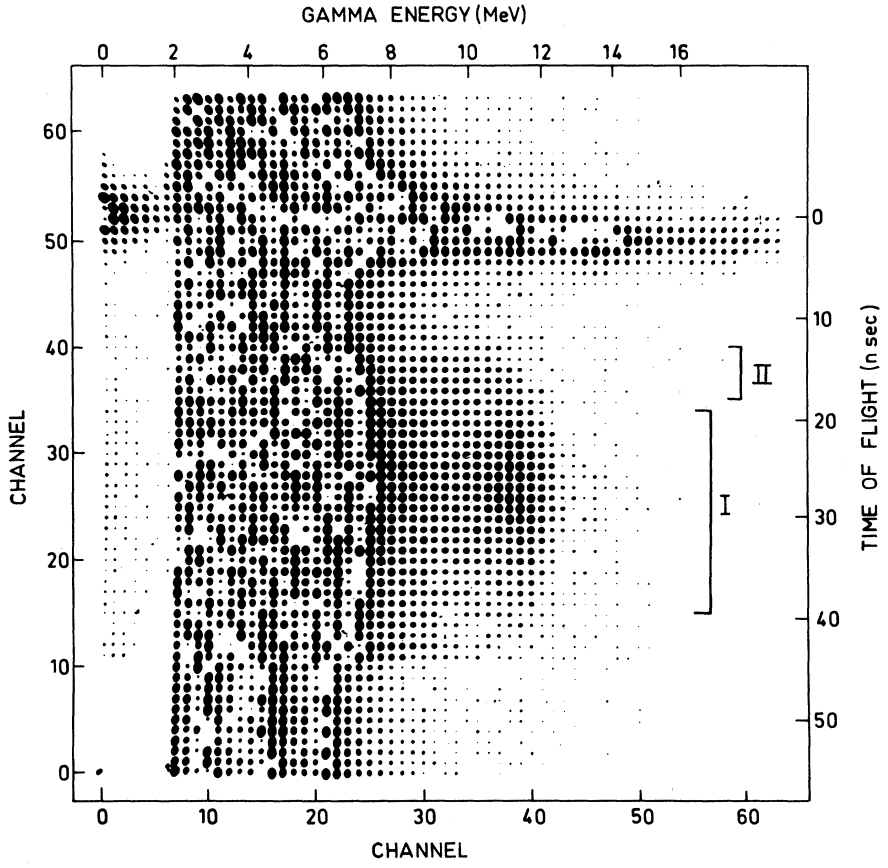


FIG. 8. Neutron time-of-flight versus $\gamma$ energy spectrum from $^7$Li+$^3$He, $E(^3\text{He}) = 7.5$ MeV, $\theta_n = 0°$, $\theta_\gamma = 125°$. The line appearing around flight-time channel 50 is the $\gamma$-$\gamma$ line due to interactions between neutron and $\gamma$ counter. Events from the sequence $^7$Li($^3$He,$p$)$^9$Be(14.39 MeV)($\gamma$)$^9$Be(2.43)($\alpha + \alpha + n$) are in region I. The flight path is 34.2 cm.

flight axis. The shape of the center-of-mass neutron spectrum from the decay of the 2.43-MeV state in $^9$Be is known from the work of CTK.[16] We have calculated the expected neutron distribution in our case using their published neutron spectrum, folding in the $^9$Be recoil effect mentioned above (for an isotropic center-of-mass proton distribution). The resulting spectrum, after taking into account the energy dependence of the neutron-detector efficiency, is shown as a dashed line in Fig. 10. The remaining peak centered at channel 38 is attributed to $\gamma$ decay to a state at 2.9 MeV in $^9$Be whose subsequent neutron decay is to $^8$Be(g.s.). The dash-dotted curve is the expected neutron spectrum for a level of Breit-Wigner shape, located at $E_x = 2.9$ MeV, $\Gamma = 1$ MeV in $^9$Be. (The resultant curve is very insensitive to the shape of the level.) We conclude that our spectra are well described as a sum of a transition to the 2.43-MeV state in $^9$Be and one to a state at $E_x = 2.9 \pm 0.25$ MeV of width $\Gamma = 1.0 \pm 0.25$ MeV. The ratio of $\gamma$ branches to these two states deduced from the center-of-mass neutron spectra used in producing the calculated curves of Fig. 10 yields $\Gamma_{\gamma(2.9)}/\Gamma_{\gamma(2.43)} = 0.30 \pm 0.04$.

The solid curve III of Fig. 11 was calculated using the excitation, width, and branching ratio given above.

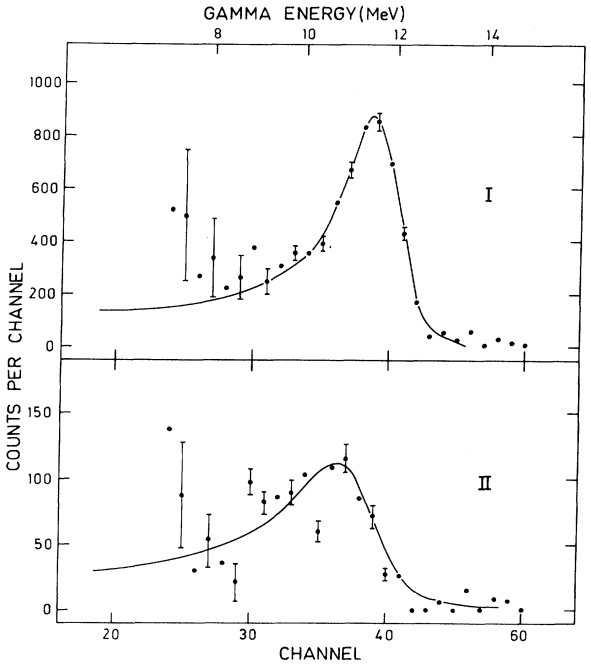


FIG. 9. High-energy portions of summed $\gamma$ spectra in regions I and II of Fig. 8. Solid curve of I is a standard shape for a $\gamma$ ray of (14.39–2.43) MeV. Solid curve of II is calculated for a $\gamma$ ray of (14.39–2.9) MeV and a width of 1 MeV for the 2.9-MeV state in $^9$Be.

There are several possible errors of principle with which one must deal before stating that the $\gamma$ decay to the 2.9-MeV "state" represent decay to the $\frac{1}{2}^-$ level. First, there may be decay to the $\frac{5}{2}^+$ level present, in spite of this transition being configurationally forbidden. The narrow width ($\Gamma = 265$ keV)[17] of this level precludes description of our results in terms of decay to this state alone. Both Figs. 9(II) and 10 require that the lower state have a width of the order of 1 MeV. By pessimistically assuming that the decay we observe is feeding both the $\frac{5}{2}^+$ state and a state at 2.65 MeV with $\Gamma = 0.75$ MeV, we deduce that $\Gamma_{\gamma(3.03)}/\Gamma_{\gamma(2.65)} = 1.3$. This may be taken as an approximative upper limit to the contribution of the $\frac{5}{2}^+$ to our spectrum. In the following discussion we have assumed that this contribution is zero. Credence is lent to this assumption by our inability to observe any decay to the $\frac{1}{2}^+$ state at 1.67 MeV, as this transition is similarly forbidden only configurationally. We stress, however, that our discarding of this possible decay mode is at the moment not required by the experimental data.

Second, if the 2.9-MeV level has appreciable decay through $^8$Be($2^+$) or $^5$He, the intensity ratio given above will have to be increased in favor of the 2.9-MeV level. The neutrons from such a decay mode would lie in region I of Fig. 8. A large contribution from this mode would be apparent in Fig. 9(I). From this spectrum we place an upper limit of 38% on the ratio of decays of the 2.9-MeV level in $^9$Be to $^8$Be($2^+$) or $^5$He to those to $^8$Be(g.s.).

If the $\gamma$ decay of the 14.39-MeV level in $^9$Be to the $\frac{5}{2}^+$ state is zero, and if the $^9$Be($\frac{1}{2}^-$, 2.9-MeV) level decays entirely to $^8$Be(g.s.), we may deduce, from $\Gamma_{\gamma 0} = 10.5$ eV and the above branching ratios, $\Gamma_{\gamma(2.9)} = 3.7 \pm 0.9$ eV.

### E. $n$-$\gamma$ Coincidence Spectra Relevant to $^9$B

In Fig. 12(a) we display an $n$-$\gamma$ spectrum taken at a bombarding energy of 8.7 MeV, 770 keV above the threshold for production of $^9$B(14.67 MeV). Experimental conditions were those described in Sec. 2 D, except for the change of bombarding energy and the use of $^7$Li($^3$He, $d$)$^8$Be(g.s.) monitor under the same conditions as in Secs. 2 A and 2 B. The horizontal line appearing in region I (time channel 10) corresponds to the sequence $^7$Li($^3$He, $n$)-$^9$B(14.67 MeV)($\gamma$)$^9$B. A projection of events from this axis on the $\gamma$-energy axis is shown in Fig. 12(b). Kinematics allow a contribution to the spectrum of Fig. 12(b) from the sequence $^7$Li($^3$He, $p$)-$^9$Be(14.39 MeV)($\gamma$)$^9$Be*($n$). Using the description of the latter sequence developed in Sec. 2 D, and normalizing to region II of Fig. 12(a), we have calculated the size and shape of this contribution, as

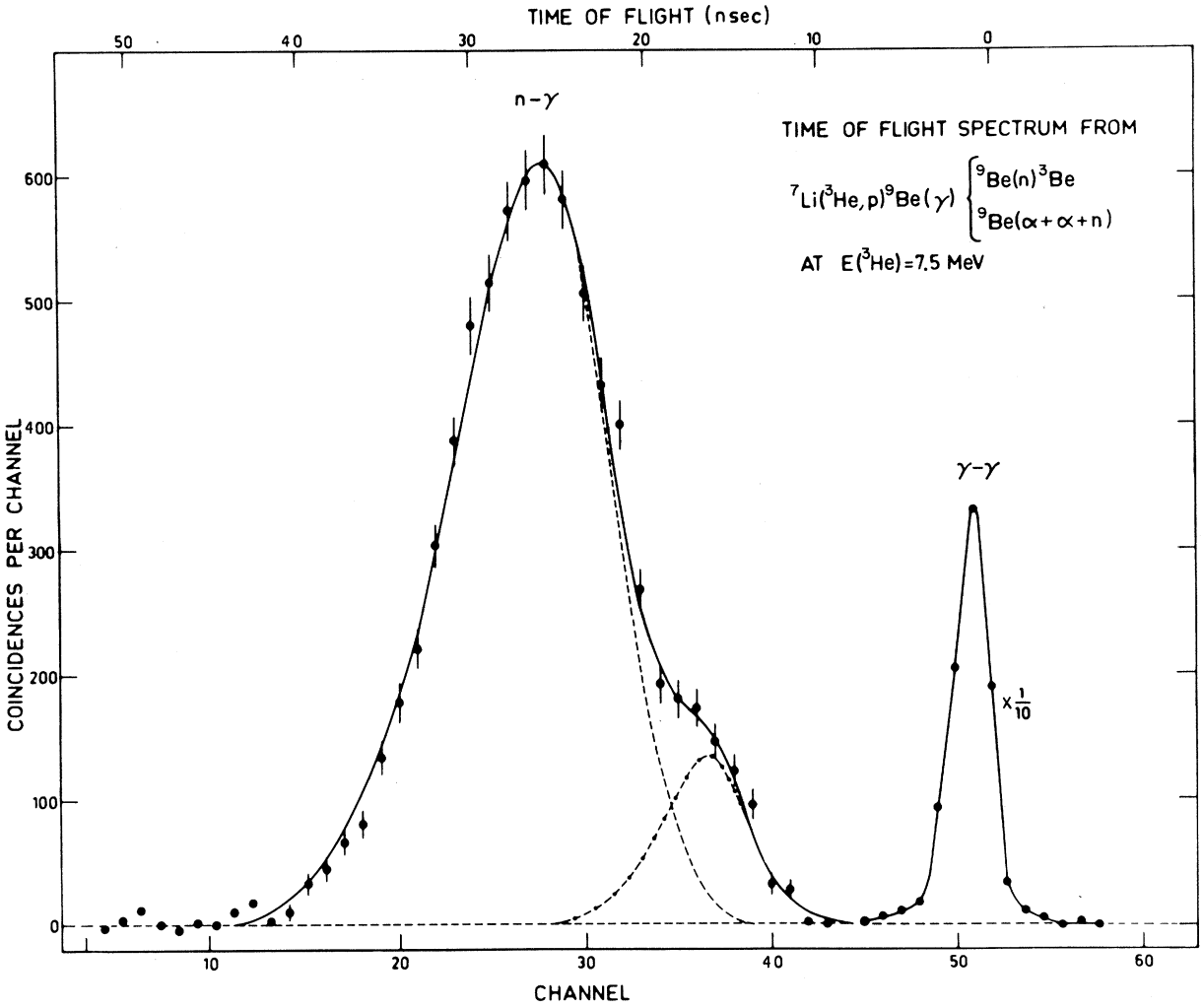


FIG. 10. Summed time-of-flight spectrum above $\gamma$-energy channel 30 of Fig. 8. The dashed curve is a calculated shape for the sequence $^7$Li($^3$He,$p$)$^9$Be(14.39 MeV)($\gamma$)$^9$Be(2.43)($\alpha+\alpha+n$) and $^9$Be(2.43)($n$)$^8$Be(g.s.) using spectrum shape of Ref. 16. The dashed dotted line is calculated for the sequence $^7$Li($^3$He,$p$)$^9$Be(14.39 MeV)($\gamma$)$^9$Be(2.9)($n$)$^8$Be(g.s.) assuming a Breit-Wigner shape ($\Gamma$=1 MeV) for the 2.9-MeV state.

shown by the dashed line in Fig. 12(b). The remaining spectrum displays $\gamma$ decays from $^9$B(14.67 MeV) only. The solid lines represent the spectrum expected from decays to levels in $^9$B at 0.0, 2.34, and 3.0 MeV ($\Gamma$=1.5 MeV) with intensities in the ratio 1, 1.19, and 0.3 as deduced from the $^9$Be (14.39 MeV) decays. We conclude that the data are in good agreement with the assumption that the branching ratios in $^9$Be and $^9$B are equal. No more detailed attempt to extract branching ratios from $^9$B(14.56 MeV) spectrum was made.

In the absence of a singles neutron spectrum the method used to extract $\Gamma_{\gamma 0}/\Gamma_{tot}$ for $^9$Be(14.39 MeV) (see Sec. 2B) could not be used for $^9$B(14.67 MeV). Instead two alternative, but inherently less precise, methods were used

(1) Absolute differential cross sections at $\theta=0°$ for the reactions $^7$Li($^3$He, $p$)$^9$Be(14.39 MeV) at $E(^3\text{He})=10$ MeV and $^7$Li($^3$He, $n$)$^9$B(14.67 MeV) at $E(^3\text{He})=8.7$ MeV have been found to be $1.15^{+0.57\ 19}_{-0.34}$ and $1.63\pm0.21$ mb/sr,[21] respectively. In order to use it as a monitor of ($^7$Li target thickness)$\times$(total charge), the yield of $^7$Li($^3$He, $d$)$^8$Be(g.s.), $\theta_d=140°$ was measured using same target and same total beam charge at $E(^3\text{He})=10$ MeV and 8.7 MeV. The ratio of $p$-$\gamma_0$ and $n$-$\gamma_0$ coincidence yields obtained, respectively, in Sec. 2A and in this section for equivalent values of ($^7$Li target thickness)$\times$(total charge) are related by

$$\frac{Y(n\text{-}\gamma 0)}{Y(p\text{-}\gamma 0)}=\frac{d\sigma/d\Omega(^9\text{B})}{d\sigma/d\Omega(^9\text{Be})}\times\frac{\Gamma_{\gamma 0}/\Gamma_{tot}(^9\text{B})}{\Gamma_{\gamma 0}/\Gamma_{tot}(^9\text{Be})}\times\frac{\Delta\Omega_n\times\epsilon_n}{\Delta\Omega_p}.$$

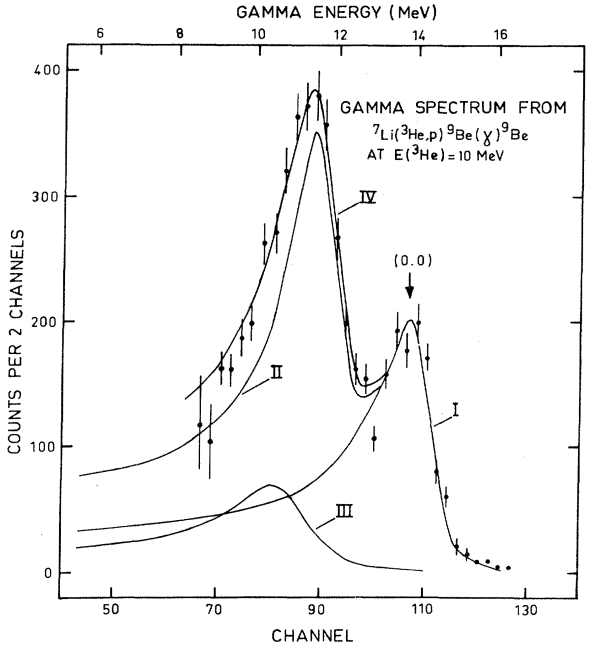


FIG. 11. $\gamma$ spectrum of Fig. 2(b). Curve II is deduced from branching ratio measurement of Sec. 2 C. Curve III is obtained using results of Sec. 2 D. Curve IV is curves (I+II)+III.

The intrinsic neutron efficiency, $\epsilon_n$, was calculated following Cocke.[22] Our results were

$$\frac{\Gamma_{\gamma 0}/\Gamma_{\mathrm{tot}}(^{9}\mathrm{B})}{\Gamma_{\gamma 0}/\Gamma_{\mathrm{tot}}(^{9}\mathrm{Be})} = 1.14^{+0.63}_{-0.34}.$$

(2) Using the description developed in Sec. 2 D for the sequence $^{7}$Li($^{3}$He,$p$)$^{9}$Be(14.39 MeV)($\gamma$)$^{9}$Be*($n$), the $\gamma$(2.43)-$n$ coincidence efficiency for this process is calculated for a bombarding energy of 8.7 MeV assuming isotropic $\gamma$(2.43)-$n$ angular correlation in the $^{9}$Be* system. By comparing yields in regions I and II of Fig. 12(a) and using the calculated $\gamma$-$n$ efficiencies, we find at $E(^{3}\mathrm{He})$ = 8.7 MeV

$$\frac{\Gamma_{\gamma(2.33)}/\Gamma_{\mathrm{tot}}(^{9}\mathrm{B})}{\Gamma_{\gamma(2.43)}/\Gamma_{\mathrm{tot}}(^{9}\mathrm{Be})} \times \frac{\sigma_{\mathrm{tot}}(^{9}\mathrm{B})}{\sigma_{\mathrm{tot}}(^{9}\mathrm{Be})} = 1.33 \pm 0.4.$$

This method has the advantage that only the relative neutron-detector efficiency as a function of neutron energy enters the calculation, the absolute-efficiency normalizing factor and detector solid angles being the same for $n$-$\gamma$ events associated with $^{9}$B production as for $^{9}$Be production.

The total cross section for the production of $^{9}$Be(14.39 MeV) has not been measured explicitly at 8.7 MeV. Measurements of $\sigma_{\mathrm{tot}}(^{9}\mathrm{Be})$ at 7.5 and 10 MeV,[19] and of $\sigma_{\mathrm{tot}}(^{9}\mathrm{B})$ at 8.7 MeV[21] indicate that $\sigma_{\mathrm{tot}}(^{9}\mathrm{B})/\sigma_{\mathrm{tot}}(^{9}\mathrm{Be})$ is near unity at 8.7 MeV. Taking this value for the cross section ratio yields

$$\frac{\Gamma_{\gamma(2.33)}/\Gamma_{\mathrm{tot}}(^{9}\mathrm{B})}{\Gamma_{\gamma(2.43)}/\Gamma_{\mathrm{tot}}(^{9}\mathrm{Be})} = 1.33 \pm 0.4.$$

Absolute normalization for the $\gamma$-decay widths is available only for $^{9}$Be, for which $\Gamma_{\gamma 0} = 10.5 \pm 1.5$ eV.[18] To the extent that the isospin of the states involved is pure, the radiative widths in $^{9}$B should, apart from the energy factor, be equal to corresponding ones in $^{9}$Be. Experiment confirms this prediction in the case of $A$ = 13 (Refs. 4–7). The spectra presented here are furthermore quite consistent with equivalent branching ratios in $^{9}$Be and $^{9}$B. We thus consider it extremely likely that $\Gamma_{\gamma(2.43)}$ for $^{9}$Be is nearly equal to $\Gamma_{\gamma(2.33)}$ for $^{9}$B. If one assumes that these widths are exactly equal, one obtains, from an average of the above ratios, the ratio of total widths for $^{9}$Be(14.39 MeV) and $^{9}$B(14.67 MeV)

$$\frac{\Gamma_{\mathrm{tot}}(^{9}\mathrm{Be})}{\Gamma_{\mathrm{tot}}(^{9}\mathrm{B})} = 1.23^{+0.54}_{-0.43}.$$

When combined with $\Gamma_{\mathrm{tot}}(^{9}\mathrm{Be}) = 0.5 \pm 0.1$ keV, this gives $\Gamma_{\mathrm{tot}}(^{9}\mathrm{B}) = 0.4^{+0.14}_{-0.18}$ keV.

## 3. DISCUSSION

Table I summarizes information on the first $T = \frac{3}{2}$ state in $^{9}$Be obtained from this experiment. A detailed comparison of the $\gamma$-decay properties of the first $T = \frac{3}{2}$ state in $^{9}$Be and the $\beta$-decay properties of the analogous $^{9}$Li ground state with shell-model calculations of Barker[14] and Cohen and Kurath[13] is made in Table II. It has been pointed out by Cohen and Kurath that weak $\beta$-decay matrix elements, with which we are dealing in this case, are especially sensitive to details of the wave functions. Small discrepancies between theory and experiment are therefore not surprising. One might hope for somewhat better agreement in the case of the $\gamma$ transitions.

It is tempting to compare the experimental $M1$ $\gamma$-decay strengths with the analog Gamow-Teller $\beta$-decay transitions from the $^{9}$Li ground state. The column headed "$\beta$" in Table II displays the spin contribution to the $M1$ transition probability calculated from the corresponding experimental $\beta$-transition probabilities,[16] using $\Lambda(M1) = 7.4\Lambda(GT)$.[23] Hanna has previously noted that this contribution fails badly to account for the observed $\gamma$ strengths in $A$ = 9 and that the "orbital" contribution to the $M1$ $\gamma$ decay appears to play an important role in these transitions.[23] Dietrich *et al.*[4] have pointed out the dangers of ignoring this orbital contribution in the case of the first $T = \frac{3}{2}$ states in $A$ = 13. The comparison made in Table II fully supports these conclusions and indicates that a detailed model calculation must be used to account simultan-

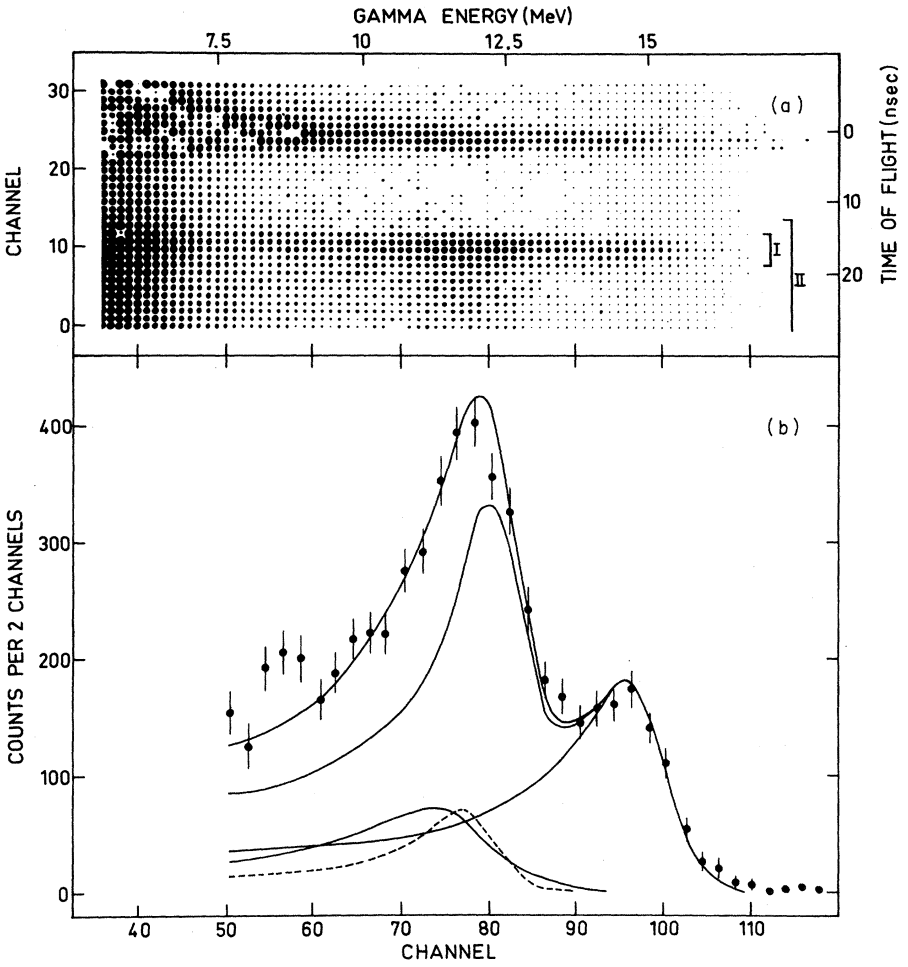


FIG. 12. (a) Neutron time-of-flight vs $\gamma$ energy from $^7$Li + $^3$He, $E(^3\text{He}) = 8.7$ MeV, $\theta_n = 0°$, $\theta_\gamma = 125°$. The flight path is 34 cm. Events from $^7\text{Li}(^3\text{He},n)^9\text{B}(14.67\text{ MeV})(\gamma)$ are in region I. Events from $^7\text{Li}(^3\text{He},p)^9\text{Be}(14.39\text{ MeV})(\gamma)^9\text{Be}^*(n)$ are in region II (see Sec. 2 D). (b) High-energy portion of summed $\gamma$ spectrum in region I of (a). The dashed curve is the contribution of the $^9$Be decays in this spectrum. Solid curves are calculated using the same branching ratios as for Fig. 11.

eously for the $\beta$- and $\gamma$-decay strengths.

Our comparison of the $\gamma$ spectra from the first $T = \frac{3}{2}$ states in $^9$Be and $^9$B show consistency with the mirror symmetry of the decay schemes expected if both the $T = \frac{3}{2}$ and $T = \frac{1}{2}$ states are isospin pure. As discussed previously,[5] however, the small values for $\Gamma_{\text{tot}}$ for these states place a more stringent limit on the size of possible isospin impurities in the $T = \frac{3}{2}$ wave functions than does the comparison of mirror $\gamma$-decay schemes until the latter comparison can be made experimentally with an accuracy at least 5%.

Barker has calculated the Coulomb-mixing matrix element between his $(3,2)^2\text{P}$, $T = \frac{1}{2}$ state at 12.76 MeV and the first $T = \frac{3}{2}$ state at 14.39 MeV to be 19 keV.[24] It is entertaining to speculate that mixing of these two states may be a primary contributor to the total width $\Gamma_{\text{tot}} = 0.5 \pm 0.1$ keV observed for the 14.39-MeV state. If one identifies the 13.72-MeV state ($\Gamma = 600$ keV)[17] with the $(3,2)^2\text{P}$ shell-model state, the expected contribution to the total width of the $T = \frac{3}{2}$ level due to this mixing should be approximately

$$\left[\frac{19\times 10^{-3}\text{ MeV}}{14.39-13.72\text{ MeV}}\right]^2 \times (600\text{ keV}) \simeq 0.5\text{ keV},$$

in fortuitously good agreement with the observed width. Barker further finds that the Coulomb matrix elements between $T = \frac{3}{2}$ and $T = \frac{1}{2}$ shell-model states are systematically smaller in the $^9$B than in $^9$Be. In the case of $^{13}$N, this mixing is identically zero, since there is only one proton hole in the $p$ shell and the two-body Coulomb operator must act between protons. The observed width[5] of

TABLE I. Experimental results for the first $T=\frac{3}{2}$ level in $^9$Be.

| $^9$Be | This work | Other authors |
|---|---|---|
| $\frac{\Gamma_{\gamma 0}(14.39\rightarrow 0)}{\Gamma_{tot}}$ | $0.021\pm0.004$ | $0.023\pm0.005$ [a] |
| $\frac{\Gamma_{\gamma(2.43)}(14.39\rightarrow 2.43)}{\Gamma_{tot}}$ | $0.025\pm0.006$ [b] | $0.04\pm0.01$ [a] |
| $\frac{\Gamma_{\gamma(2.43)}(14.39\rightarrow 2.43)}{\Gamma_{tot}}$ | $1.19\pm0.16$ | |
| $\frac{\Gamma_{\gamma(2.9+3.03)}(14.39\rightarrow 2.9+3.03)}{\Gamma_{\gamma(2.43)}(14.39\rightarrow 2.43)}$ | $0.30\pm0.04$ | |
| $\Gamma_{\gamma 0}$ (eV) | | $10.5\pm1.5$ [c]<br>18 [d] |
| $\Gamma_{tot}$ (keV) | $0.50\pm0.1$ [f] | 0.8 [e]<br>$0.46\pm0.17$ [c] |
| $\Gamma_{\gamma(2.43)}$ (eV) | $12.5\pm2.5$ [f] | |
| $\Gamma_{\gamma(2.9+3.03)}$ (eV) | $3.7\pm0.9$ [f] | |
| $\frac{\Gamma_{\alpha}(2.9\rightarrow\alpha+\alpha+n)}{\Gamma_n[2.9\rightarrow{}^8\mathrm{Be}(0)]}$ | $\leq 0.38$ | $\leq 0.60$ [g] |

[a] Ref. 3.
[b] Our result obtained by combining $\Gamma_{tot}=(0.5\pm0.1)$ keV and $\Gamma_{\gamma(2.43)}=(12.5\pm2.5)$ eV.
[c] Ref. 18.
[d] R. D. Edge and G. A. Peterson, Phys. Rev. 128, 2750 (1962).
[e] Ref. 17.
[f] Our result assuming $\Gamma_{\gamma 0}(M1)=(10.5\pm1.5)$ eV (Ref. 18).
[g] Ref. 16.

TABLE II. Comparison of $\Lambda(M1)$ experimental and theoretical values for the $^9$Be (14.39 MeV; $\frac{3}{2}^-$; $\frac{3}{2}$) state.

| Final state MeV | $J^\pi$ | $T$ | $\Gamma_\gamma$ (eV) | $\Lambda(M1)$ Exp. | $\Lambda(M1)$ Barker (Ref. 14) | $\Lambda(M1)$ Cohen-Kurath (Ref. 13) | "$\beta$" |
|---|---|---|---|---|---|---|---|
| 0 | $\frac{3}{2}^-$ | $\frac{1}{2}$ | $10.5\pm1.5$ [a] | 1.3 | 0.63 | 1.31 | 0.25 |
| 2.43 | $\frac{5}{2}^-$ | $\frac{1}{2}$ | $12.5\pm2.5$ [b] | 2.6 | 1.05 | 1.20 | 0.33 |
| 2.9 | $(\frac{1}{2}^-)$ | $\frac{1}{2}$ | $3.7\pm0.9$ [b] | 0.9 | 0.10 | 0.50 | 0.03 |

[a] Ref. 18.
[b] Our result assuming $\Gamma_{\gamma 0}(M1)=10.5\pm1.5$ eV.

the first $T=\frac{3}{2}$ state of $^{13}$N($\Gamma=1.13\pm0.3$ keV) is less than that of $^{13}$C($\Gamma=4.7\pm1.6$ keV). The nonzero width for $^{13}$N could perhaps be attributed to deficiency of the simple shell-model description or to $T=1$ admixtures in low-lying states of $^{12}$C.

Our present results indicate that the width of the first $T=\frac{3}{2}$ state in $^9$B is about 80% of that in $^9$Be within large experimental errors, however. Barker[24] finds the size of the Coulomb matrix element between his $(3,2)^2$P, $T=\frac{1}{2}$ state and the $T=\frac{3}{2}$ state to be only 5 keV in the case of $^9$B. If one estimates the total width of $^9$B(14.67 MeV) to be less than that of $^9$Be(14.39 MeV) in the ratio of the square of (5 keV)/(19 keV), one finds the width of the $^9$B state to be only 0.035 keV, to be compared with the experimental value of 0.4 keV. Both the $A=9$ and $A=13$ results give the larger width to the neutron-rich twin, in the same direction as Coulomb-mixing calculations indicate, although the size of the effect is not outside the experimental errors bars in the case of $A=9$. We conclude that the variation with $T_Z$ of the total widths of the first $T=\frac{3}{2}$ states in $A=9$ and $A=13$ may be due to the $T_z$ dependence of the Coulomb matrix-elements mixing states with neighboring states having $T=\frac{1}{2}$ and the same spin and parity, but that a better understanding of $T=\frac{1}{2}$ states in the region of the $T=\frac{3}{2}$ levels will be required before a more quantitative conclusion is possible.

## ACKNOWLEDGMENTS

We would like to thank Dr. F. C. Barker for communicating to us his Coulomb-mixing calculations

and Dr. Y. S. Chen, Dr. T. A. Tombrello, and Dr. R. W. Kavanagh for sending us their $^9$Li results prior to publication. One of us (C.L.C.) acknowledges financial support from the Institut de Recherches Nucléaires. He especially wishes to express his thanks to Dr. S. Gorodetsky and Dr. P. Chevallier for making his stay at Strasbourg a profitable and enjoyable one.

---

*Present address: Kansas State University, Manhattan, Kansas.

†National Science Foundation Postdoctoral Fellow, 1968–1969.

[1]E. G. Adelberger, C. L. Cocke, C. N. Davids, and A. B. McDonald, Phys. Rev. Letters 22, 352 (1969).

[2]A. B. McDonald, E. G. Adelberger, H. B. Mak, D. Ashery, A. P. Shukla, C. L. Cocke, and C. N. Davids, Phys. Letters 31B, 119 (1970).

[3]G. M. Griffiths, Nucl. Phys. 65, 647 (1965).

[4]F. S. Dietrich, M. Suffert, A. V. Nero, and S. S. Hanna, Phys. Rev. 168, 1169 (1968).

[5]C. L. Cocke, J. C. Adloff, and P. Chevallier, Phys. Rev. 176, 1120 (1968).

[6]G. A. Peterson, Phys. Letters 25B, 549 (1967).

[7]G. Wittwer, H. G. Clerc, and G. A. Beer, Phys. Letters 30B, 634 (1969).

[8]E. K. Warburton and J. Weneser, in *Isospin in Nuclear Physics*, edited by D. H. Wilkinson (North-Holland Publishing Company, Amsterdam, The Netherlands, 1969), p. 173.

[9]G. M. Temmer, B. Teitelmann, R. Van Bree, and H. Ogato, J. Phys. Soc. Japan Suppl. 24, 299 (1968).

[10]M. J. Le Vine and P. D. Parker, Phys. Rev. 186, 1021 (1969).

[11]K. A. Snower, E. G. Adelberger, and F. Riess, Bull. Am. Phys. Soc. 13, 1662 (1968).

[12]A. Amit and A. Katz, Nucl. Phys. 58, 388 (1964).

[13]S. Cohen and D. Kurath, Nucl. Phys. 73, 1 (1965).

[14]F. C. Barker, Nucl. Phys. 83, 418 (1966).

[15]B. E. F. Macefield, B. Wakefield, and D. H. Wilkinson, Nucl. Phys. A131, 136 (1969).

[16]Y. S. Chen, T. A. Tombrello, and R. W. Kavanagh, Nucl. Phys. A146, 136 (1970).

[17]T. Lauritsen and F. Ajzenberg-Selove, Nucl. Phys. 78, 1 (1966).

[18]H. G. Clerc, K. J. Wetzel, and E. Spamer, Phys. Letters 20, 667 (1966).

[19]B. Lynch, G. M. Griffiths, and T. Lauritsen, Nucl. Phys. 65, 641 (1965).

[20]P. R. Christensen and C. L. Cocke, Nucl. Phys. 89, 656 (1966).

[21]F. S. Dietrich, Nucl. Phys. 69, 49 (1965).

[22]C. L. Cocke, Ph.D. thesis, California Institute of Technology, Pasadena, California, 1967 (unpublished).

[23]S. S. Hanna, in *Isospin in Nuclear Physics*, edited by D. H. Wilkinson (North-Holland Publishing Company, Amsterdam, The Netherlands, 1969), p. 591.

[24]F. C. Barker, private communication.

---

PHYSICAL REVIEW C VOLUME 3, NUMBER 5 MAY 1971

# Excitation of $^{20}$Ne by 180° Electron Scattering

W. L. Bendel, L. W. Fagg, S. K. Numrich,* E. C. Jones, Jr., and H. F. Kaiser

*Nuclear Physics Division, Naval Research Laboratory, Washington, D. C. 20390*

(Received 10 December 1970)

States in $^{20}$Ne have been studied by 180° inelastic electron scattering with incident energies of 39 and 56 MeV. A large scattering peak is found at each bombarding energy, showing excitation of a $1^+$, $T=1$ state at 11.2 MeV, with transition radius $R = 2.53 \pm 0.15$ fm and radiation width $\Gamma_0 = 11 \pm 2$ eV. Other levels from 11 to 19 MeV are also excited.

## I. INTRODUCTION

Electron scattering at 180° has proven particularly useful in exciting $1^+$, $T=1$ states in even-even $T=0$ nuclei. As electric transitions are inhibited at 180°, magnetic transitions generally dominate, particularly magnetic dipole ($M1$) transitions. Inhibition of $\Delta T = 0$, $M1$ transitions[1] in these nuclei further increases the selectivity of observable peaks in 180° scattering data. The states most abundantly excited are thus $1^+$, $T=1$ states, the analogs of low-lying states in isobaric nuclei. In addition, Kurath[2] has shown that the transition strength is concentrated in the lowest few such levels. Previous work[3,4] at 180° with $^{24}$Mg and $^{28}$Si has shown agreement with these predictions.

Preliminary results[5] on $^{20}$Ne exhibited striking concentration of the strength into one level at 11.2 MeV. In this paper, we report data on 39- and 56-MeV electron scattering from $^{20}$Ne up to an excitation energy of 20 MeV. These data are employed